



PERGAMON

Available online at www.sciencedirect.com

SCIENCE @ DIRECT®

Deep-Sea Research I 50 (2003) 417–434

DEEP-SEA RESEARCH
PART I

www.elsevier.com/locate/dsr

Phytoplankton natural fluorescence variability in the Sargasso Sea

T.K. Westberry*, D.A. Siegel

Institute for Computational Earth System Science, University of California, Santa Barbara, Santa Barbara, CA 93106-3060, USA

Received 10 October 2001; received in revised form 3 September 2002; accepted 22 January 2003

Abstract

Phytoplankton fluorescence has been used historically as a means of assessing phytoplankton biomass, rates of primary production (PP) and physiological status in laboratory, in situ, and satellite based investigations. Assumptions about the quantum yield of phytoplankton fluorescence, ϕ_f , are often overlooked and can become problematic when fluorescence based methods are applied. A time series of ϕ_f observations from the northwestern Sargasso Sea is presented with the goal of understanding the controls on fluorescence and its applicability for assessing upper ocean biological processes. Accurate estimates of ϕ_f require accounting for Raman scattering and the conversion of planar to scalar irradiance. Variability in ϕ_f occurs on both seasonal and episodic time scales. Seasonal variations show maxima in the surface layer during summer months while lower, more uniform values are found throughout the winter when deep mixing occurs. Large episodic variations in ϕ_f are observed throughout the record which dwarf seasonal changes. Predictions of depth-dependent and depth-integrated PP rates using ϕ_f and natural fluorescence fluxes are only marginally successful ($r^2 \sim 50\%$), although comparable with results from global bio-optical models for the Sargasso Sea. Improvements in PP predictions are hindered by weak statistical relationships with other parameters. ϕ_f is largely decoupled from the quantum yield of carbon assimilation, ϕ_c , indicating that an inverse relationship between fluorescence and photosynthesis does not exist. Consequently, variability in the quantum yield of thermal de-excitation, ϕ_h , is found to be of similar magnitude as ϕ_f on the timescales observed. These observations show that assumptions about photochemical energy flow through the phytoplankton community must be made carefully and that the fluorescence–photosynthesis relationship is not straightforward.

© 2003 Elsevier Science Ltd. All rights reserved.

Keywords: Fluorescence; Quantum yield; Sargasso Sea

1. Introduction

The fluorescence signal emitted by a phytoplankton assemblage contains a wealth of information on its light history, nutritional status,

photosynthetic capacity and community composition. Solar-stimulated, or “natural” fluorescence is a passive measurement of this signal that provides relatively easy, non-intrusive estimates of some of these processes on a wide range of spatial and temporal scales (e.g., Kiefer et al., 1989; Letelier and Abbott, 1996; Waters and Smith, 1994). Fluorescence has long been used to assess phytoplankton pigment biomass in both in situ and laboratory environments (Lorenzen, 1966;

*Corresponding author. Institute for Computational Earth System Science, University of California, Santa Barbara, Santa Barbara, CA 93106-3060, USA. Fax: +1-805-893-2578.

E-mail address: toby@icess.ucsb.edu (T.K. Westberry).

Strickland and Parsons, 1968). Its quantitative application requires knowledge of the quantum yield of fluorescence, ϕ_f , and the factors controlling its variations. Despite widespread application, little is known about the scales of variability for ϕ_f and it is often treated as a constant. Further, the use of fluorescence to derive information about photosynthetic rates is complicated by the fact that the signal is not a simple linear function of chlorophyll concentration or photosynthetic activity (Falkowski and Kiefer, 1985; Kiefer et al., 1989). Nonetheless, both empirical and mechanistic relationships between fluorescence and primary production (PP) have been used with varying degrees of success over the years (Neville and Gower, 1977; Topliss and Platt, 1986; Kiefer et al., 1989; Chamberlin et al., 1990; Kiefer and Reynolds, 1992; Babin et al., 1996).

Central to the application of phytoplankton fluorescence to determinations of PP rates is the relationship between the quantum yields of carbon fixation, ϕ_c , and fluorescence, ϕ_f . These quantities can be defined by the rate of naturally fluoresced radiation, NFR ($\text{Ein m}^{-3} \text{d}^{-1}$), and the energy utilized for PP ($\text{mg C m}^{-3} \text{d}^{-1}$), normalized by the quanta absorbed by phytoplankton, AQ ($\text{Ein m}^{-3} \text{d}^{-1}$):

$$\phi_f(z) = \frac{\text{NFR}(z)}{\text{AQ}(z)}, \quad (1a)$$

$$\phi_c(z) = \frac{\text{PP}(z)}{\text{AQ}(z)}. \quad (1b)$$

The units of ϕ_f and ϕ_c are Einstein fluoresced/Einstein absorbed (sometimes reported as dimensionless) and mol C/Einstein, respectively. The two expressions above can be combined to express the rate of PP in terms of NFR and the ratio of the quantum yields, ϕ_c/ϕ_f (Chamberlin et al., 1990; Kiefer and Reynolds, 1992). However, in order to apply this formulation it must also be assumed that ϕ_c/ϕ_f is constant or behaves in a predictable manner (i.e., Chamberlin et al., 1990; Chamberlin and Marra, 1992).

Estimates of ϕ_f are also used as a composite index of phytoplankton “health”, reflecting nutrient availability, physiological status and species composition (Falkowski and Kolber, 1995; Lete-

lier et al., 1997). Numerous biophysical models and observations suggest that an inverse relationship exists between ϕ_f and ϕ_c , demonstrating a competition between fluorescence and photosynthesis for absorbed light energy (Butler, 1966; Topliss and Platt, 1986; Owens, 1991; Kiefer and Reynolds, 1992; Garcia-Mendoza and Maske, 1996). Diversion of light energy for photosynthetic processes is termed photochemical quenching of fluorescence. However, the majority of absorbed radiation is not used to drive photosynthesis or fluorescence, but is transferred away from the cell in the form of heat, a process collectively called thermal deactivation or non-radiative dissipation. The processes that result in thermal deactivation are many and include cycling of xanthophylls, state transitions, accumulation of a pH gradient across the thylakoid membrane, and others (Owens, 1991; Krause and Weiss, 1991; Kiefer and Reynolds, 1992; Olaizola et al., 1994). It follows, then, that the efficiency with which these processes collectively dissipate absorbed radiant energy be referred to as the quantum yield of heat production, ϕ_h . Thus, fluorescence and photosynthesis are only two out of three possible end products of absorbed radiation, and in order for a predictable inverse relationship between ϕ_f and ϕ_c to exist, ϕ_h must remain constant.

In this paper we utilize an extensive bio-optical dataset taken from the Bermuda Atlantic Time Series Study (BATS) in the northwestern Sargasso Sea to address these assumptions and applications of ϕ_f on a variety of timescales. Using fluorescence fluxes calculated from radiative transfer principles we compute quantum yields for fluorescence and use these to model PP rates. We also show that the processes regulating ϕ_f and ϕ_c are decoupled. That is, ϕ_f and ϕ_c are operating independently of one another despite shared environmental forcings. This has important implications for interpretation of phytoplankton physiology based upon field determinations of fluorescent properties.

2. Methods

Data presented here were collected as part of the concurrent Bermuda Bio-Optics Program

(BBOP) and BATS sampling programs during the period January 1992 to December 1997. The BATS site is ~ 80 km southeast of the island of Bermuda ($31^{\circ}50'N$, $64^{\circ}10'W$) in the north-western Sargasso Sea. The site was visited on a monthly basis biweekly during the spring bloom period. The BATS sampling and analysis methods are well documented and are described only briefly here (Lohrenz et al., 1992; Knap et al., 1993; Michaels et al., 1994; Michaels and Knap, 1996; Siegel et al., 2001; Steinberg et al., 2001).

Underwater profiles of downwelling spectral irradiance, $E_d(\lambda, z, t')$, and upwelling spectral radiance, $L_u(\lambda, z, t')$, were taken from a profiling spectroradiometer (Biospherical Instruments, MER-2040, San Diego, California; Smith et al., 1984). Prior to December 1993, measurements were made at 8 discrete wavebands (410, 441, 465, 488, 520, 565, 589, 665 nm, with an additional wavelength at 683 nm on the upwelling radiance sensor). After this time 4 more channels were added at 510, 555, 625, and 683 nm (E_d only). Prior to December 1993 the gain sensitivity of the $L_u(683, z, t')$ determinations was such that values recorded below 80 m were sparse. Incident surface irradiance measurements, $E_d(\lambda, 0^+, t')$, were made simultaneously on deck (see Table 1 for description of symbols and units). A detailed calibration history has been kept on all instruments, and uncertainties for spectral irradiance are less than 0.5% over the period of interest (O'Brien et al., 2000; Sorensen and Siegel, 2001).

PP measurements were made by dawn-to-dusk in situ incubations from a freely drifting array at eight discrete depths (nominally 1, 20, 40, 60, 80, 100, 120, and 140 m). Each sample, consisting of three replicates and a dark sample, was inoculated with $^{14}HCO_3$, returned to the respective depth, and incubated through the day. All sampling and sample processing employed trace-metal clean procedures (Fitzwater et al., 1982; Knap et al., 1993).

A Sea-Bird CTD instrument package equipped with 24 12-l Niskin bottles was used for continuous profiles of temperature and salinity in the upper 500 m. Water samples were collected at 10 m intervals (0–200 m) from a near noon-time cast for

biological and chemical analyses. Four-liter samples were filtered on to 2.5 cm GF/F filters and stored in liquid nitrogen for quantification of phytoplankton pigments using reverse-phase high-performance liquid chromatography (Knap et al., 1993; Steinberg et al., 2001). Total nitrate (+ nitrite) was also measured in samples from the same depths by standard colorimetric techniques after filtration through 0.8 μm Nuclepore filters (Knap et al., 1993).

3. Calculation of absorbed quanta (AQ)

The fraction of available radiation that is absorbed by a phytoplankton assemblage over the course of a solar day, AQ, is simply the product of the wavelength dependent phytoplankton absorption coefficient, $a_{ph}(\lambda, z)$ (m^{-1}), and the spectral, quantum, scalar irradiance, $E_o(\lambda, z, t')$ ($Ein\ m^{-2}\ s^{-1}\ nm^{-1}$) integrated over the visible light spectrum and daylength:

$$AQ(PAR, z) = \int_{400}^{700} a_{ph}(\lambda, z) \times \int_{sr}^{ss} E_o(\lambda, z, t') dt' d\lambda \quad (Ein\ m^{-3}), \quad (2)$$

where t' is time during the solar day. The limits of integration are from local sunrise to sunset and over the visible domain (400–700 nm). Values of $E_o(\lambda, z, t')$ are calculated by transforming spectral downwelling irradiance above the sea surface, $E_d(\lambda, 0^+, t')$ in two ways. First, these values are propagated to depth using a mean in situ transmission profile for each cruise, $TR(\lambda, z)$, and a factor that accounts for specular reflection at the sea surface, r ($\sim 2\%$; Austin, 1974):

$$E_o(\lambda, z, t') = \frac{E_d(\lambda, 0^+, t')}{\mu'(\lambda, z, t')} \times (1 - r) \quad TR(\lambda, z) \quad (Ein\ m^{-2}\ nm^{-1}\ s^{-1}). \quad (3)$$

The spectral transmission through the water column, $TR(\lambda, z)$, is in turn defined as the ratio of the spectral downwelling irradiance at depth to that just below the surface and is calculated for all

Table 1
List of symbols and units used

Symbol	Description	Units
$a_{\text{ph}}(\lambda, z)$	Phytoplankton absorption	m^{-1}
$\text{AQ}(\text{PAR}, z)$	Absorbed broadband, quantum radiation	$\text{Ein m}^{-3} \text{d}^{-1}$
$c(\lambda, z)$	Beam attenuation coefficient	m^{-1}
$c_{\text{p}}(683, z)$	Particle beam attenuation coefficient	m^{-1}
$E_{\text{d}}(\lambda, z)$	Downwelling planar irradiance	$\text{Ein m}^{-2} \text{nm}^{-1} \text{s}^{-1}$
$E_{\text{d}}(\lambda, 0^+)$	Incident downwelling planar irradiance	$\text{Ein m}^{-2} \text{nm}^{-1} \text{s}^{-1}$
$E_{\text{o}}(\lambda, z)$	Downwelling scalar irradiance	$\text{Ein m}^{-2} \text{nm}^{-1} \text{s}^{-1}$
$L_{\text{u}}(683, z)$	Upwelling radiance at 683 nm	$\text{Ein m}^{-2} \text{s}^{-1} \text{nm}^{-1} \text{sr}^{-1}$
L_{c}^*	Elastic scatter path function	$\text{Ein m}^{-3} \text{s}^{-1} \text{nm}^{-1} \text{sr}^{-1}$
$\Delta L_{\text{u}}(683, z)$	Raman enhancement of radiance at 683 nm	$\mu \text{Ein m}^{-2} \text{s}^{-1} \text{nm}^{-1} \text{sr}^{-1}$
NFR	Naturally fluoresced radiation	$\text{Ein m}^{-3} \text{d}^{-1}$
PP(z)	Primary production rate	$\text{mg C m}^{-1} \text{d}^{-1}$
ϕ_{f}	Quantum yield of fluorescence	$\text{Ein fluoresced Ein absorbed}^{-1}$
ϕ_{c}	Quantum yield of carbon assimilation	mol C Ein^{-1}
ϕ_{h}	Quantum yield of heat production	
S_{o}	Internal source term in radiative transfer equation	$\text{Ein m}^{-3} \text{s}^{-1} \text{nm}^{-1} \text{sr}^{-1}$
$\text{TR}(\lambda, z)$	in situ irradiance transmission function	Dimensionless

vertical profiles between 9 am and 3 pm ($N \sim 10$). This approach is required because the underwater irradiance field is only measured during the individual profiles, while the incident irradiance, $E_{\text{d}}(\lambda, 0^+, t')$, is measured continuously throughout the day.

Secondly, a geometric correction was applied, which allowed for the direct conversion of downwelling planar irradiance to scalar irradiance:

$$\mu'(\lambda, z, t', \text{chl}) = \frac{E_{\text{d}}(\lambda, z, t')}{E_{\text{o}}(\lambda, z, t')}, \quad (4)$$

where μ' is a parameter similar to the mean cosine, μ (Westberry, 2001). Values of μ' were generated with an underwater radiative transfer model (HYDROLIGHT 4.1, see Mobley, 1994 for model details) over a range of wavelengths (400–700 nm), chlorophyll concentrations (0.01 – 1.0 mg m^{-3}), and depths (0–50 m) (Fig. 1). Generally, this quantity behaved similarly to the mean cosine (e.g., Bannister, 1992; Berwald et al., 1995), but the magnitudes were significantly different. Depth variations in μ' were negligible below ~ 20 m (not shown). As no data shallower than 20 m are used in this analysis (discussed later) a mean μ' spectrum averaged between 20 and 50 m was used. The remaining wavelength and chlorophyll-dependent variability is accounted for by interpolating within a 2-D lookup table based on Fig. 1.

Phytoplankton absorption spectra, $a_{\text{ph}}(\lambda, z)$, were spectrally reconstructed following Bidigare et al. (1990) using known in vivo absorption coefficients and class specific pigment concentrations from a noon-time cast. Individual pigment concentrations were grouped into one of five pigment classes (chlorophyll *a*, *b*, *c*, photosynthetic carotenoids, and photoprotective carotenoids) and summed to give the total absorption by the phytoplankton community, $a_{\text{ph}}(\lambda)$. Potential errors of this method—including contributions due to phycobilipigments and pigment packaging effects—as applied to this site have been addressed elsewhere (Bidigare et al., 1990; Sorensen and Siegel, 2001).

Estimates of ϕ_{c} were subsequently calculated by normalizing the dawn-to-dusk PP rates by the daily, average absorbed broadband quanta (Eq. (1a)). Thus, these values represent an effective or operational quantum yield, not an instantaneous or physiological quantum yield (Sorensen and Siegel, 2001).

4. Calculation of NFR

An empirical model was developed in order to construct a near-continuous record of upwelling radiance at 683 nm over the course of a day $L_{\text{u}}(683, z, t')$ ($\text{Ein m}^{-2} \text{s}^{-1} \text{nm}^{-1} \text{sr}^{-1}$). The model

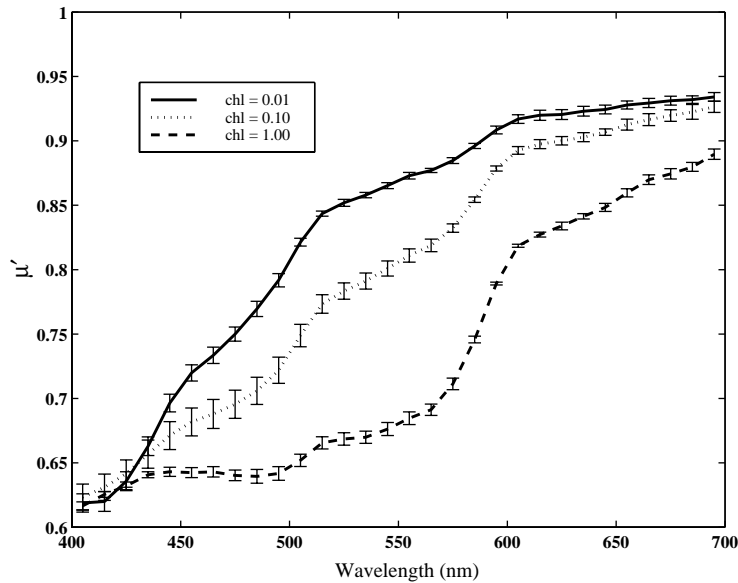


Fig. 1. The quantity μ' allows for the conversion of planar irradiance to scalar irradiance. Shown is μ' evaluated within HYDROLIGHT 4.1 for a range of chlorophyll concentrations (mg m^{-3}). For each chlorophyll level, the mean spectrum for depths between 20 and 50 m is shown with 1σ error-bars.

assumes a constant relationship between $L_u(683, z, t')$, which is measured only during radiometer profiles, and $E_d(488, 0^+, t')$, which is recorded continuously on deck. Cruise-mean profiles of $L_u(683, z, t')/E_d(488, 0^+, t')$ were constructed from a number of profiles, N_p ($4 < N_p < 10$), throughout the day allowing $\hat{L}_u(683, z, t')$ to be estimated:

$$\hat{L}_u(683, z, t') = \left[\frac{1}{N_p} \sum_{i=1}^{N_p} \frac{L_u(683, z, t')}{E_d(488, 0^+, t')} \right] \times E_d(488, 0^+, t') \quad (5)$$

Normalized RMS errors between measured and modeled profiles of the upwelled radiance at depth were almost always $< 10\%$ and were $< 5\%$ in more than half the profiles.

NFR was calculated by inverting the time-independent, one-dimensional, monochromatic radiative transfer equation (RTE) with daily integrated profiles of upwelled radiance at 683 nm:

$$\frac{d\hat{L}_u}{dz} = -c\hat{L}_u + S_o + L_e^* \quad (\text{Ein m}^{-3} \text{ nm}^{-1} \text{ s}^{-1} \text{ sr}^{-1}), \quad (6)$$

where \hat{L}_u is the reconstructed upwelling radiance at 683 nm at depth given by Eq. (5), c is the beam attenuation coefficient at 683 nm (m^{-1}), S_o ($\text{Ein m}^{-3} \text{ s}^{-1} \text{ nm}^{-1} \text{ sr}^{-1}$) represents both true internal source terms (i.e., fluorescence) and inelastic scattering processes such as Raman scattering, and L_e^* ($\text{Ein m}^{-3} \text{ s}^{-1} \text{ nm}^{-1} \text{ sr}^{-1}$) is the elastic scatter path function (representing all photons scattered into the direction of interest from other directions; Mobley, 1994). Knowledge of the upwelling radiance profile (\hat{L}_u), beam attenuation coefficient (c), and the path function (L_e^*) at 683 nm allows us to solve for S_o . The beam attenuation coefficient at 683 nm was estimated from values for pure water absorption and scattering (Smith and Baker, 1981) and the mean particle beam attenuation coefficient, $c_p(683, z)$, from spectral transmissometer measurements made at the BATS site (Brody, 1998). The path function for elastic scattering of $L_u(683)$, L_e^* , was assumed to be negligible below the depths where solar photons at 683 nm contribute significantly to $L_u(683)$. At these depths, elastic scatter of fluoresced radiation will be to first order uniform, resulting in a negligible path function. The source term, S_o , can then be

estimated by difference from Eq. (6). To calculate NFR the directional (sr^{-1}) and spectral (nm^{-1}) dependences of S_0 that must be accounted for. Phytoplankton fluorescence is isotropic (Gordon, 1979; Gordon et al., 1993) and is assumed to follow a Gaussian distribution centered on 683 nm with a bandwidth of ~ 25 nm (Collins et al., 1985).

The present method for computing NFR (Eq. (6)) is similar to that of Kiefer et al. (1989), whose derivation has been widely used in oceanographic studies (Waters and Smith, 1994; Abbott et al., 1995). Combining Eq. (6) with the definition of the attenuation coefficient, $K(\lambda, z)$, and incorporating the spectral and geometric considerations gives an expression nearly identical to that of Kiefer et al. (1989) for NFR. Consequently, values of NFR computed by either method are very similar (data not shown, see Westberry, 2001).

Observations shallower than 20 m were ignored in calculating $\text{NFR}(z)$, as the $L_u(683)$ signal at those depths is confounded by solar backscattered light. However, at 20 m the contribution from solar photons to $L_u(683, z, t')$ varies from 0.0007% to 0.002% of the upwelled radiance observed at the surface, depending mainly on the chlorophyll content of the water column. The maximum possible contribution from sunlight at 20 m results in an error in NFR that is less than 1 part in 10^4 (0.01%).

5. Accounting for Raman Scattering

The upwelled light measured at 683 nm includes contributions from processes other than fluorescence, the most important of which is Raman scattering. Raman scattering is a purely physical process in the ocean resulting from photons being absorbed and re-emitted by different vibrational modes of the water molecules. The resulting wavelength shift of the re-emitted photon is always towards longer wavelengths, some of which overlap the chlorophyll *a* fluorescence emission spectrum. Thus, the source term, S_0 contains both fluoresced and Raman scattered light. Although Raman scattering is difficult to measure directly,

both analytical and numerical modeling studies have properly characterized and incorporated it into the RTE (Stavn and Weidemann, 1988; Marshall and Smith, 1990; Mobley, 1994; Bartlett et al., 1998; Gordon, 1999).

The contribution of Raman scatter to the upwelling light field was estimated here with radiative transfer simulations (HYDROLIGHT 4.1). Contributions to $L_u(683, z)$ by chlorophyll fluorescence and Raman scattering were assessed from the differences between simulations including both of these processes and cases with only Raman scattering. Inputs to the simulations were specified to mimic typical conditions for the study area (i.e., zenith angle, atmospheric properties, inherent optical properties, etc.). Fig. 2a shows the percent contribution of Raman scattering to the total upwelled light at 683 nm for a series of uniform chlorophyll profiles and for the average summer (June–Sept.) and winter (Dec.–Feb.) BATS chlorophyll profiles. Raman contributions at 683 nm are near maximal near the surface during the summertime and represent $\sim 15\%$ of the total $L_u(683, z)$ signal. Values below 20 m did reach $> 15\%$ under extremely low chlorophyll conditions, but are typically less than 7% of $L_u(683, 20 \text{ m}, t')$, similar to what is found from the average winter BATS chl *a* profile.

A simple linear model was used to predict the Raman “enhancement” of $L_u(683, z, t')$ as a function of the in situ downwelling irradiance at 555 nm (Fig. 2b). The enhancement due to Raman scattering, $\Delta L_u(683, z, t')$, is a well-defined function of the exciting radiation (peak at ~ 555 nm):

$$\begin{aligned} \Delta L_u(683, z, t') = & 2.53 \times 10^{-05} E_d(555, z, t') \\ & + 7.8 \times 10^{-7} (\mu\text{Ein m}^{-2} \text{s}^{-1} \text{nm}^{-1} \text{sr}^{-1}), \end{aligned} \quad (7)$$

where $E_d(555, z, t')$ is in units of $\mu\text{Ein m}^{-2} \text{s}^{-1} \text{nm}^{-1}$. The slope and intercept of this relationship depend weakly on chlorophyll *a* concentration, but over the range of chl *a* observed at this site the mean linear regression coefficients are not significantly different (95% confidence level) from extreme chlorophyll cases found in the BATS data. This empirical correction compares well with the method of Maritorena et al. (2000) and corrected upwelling

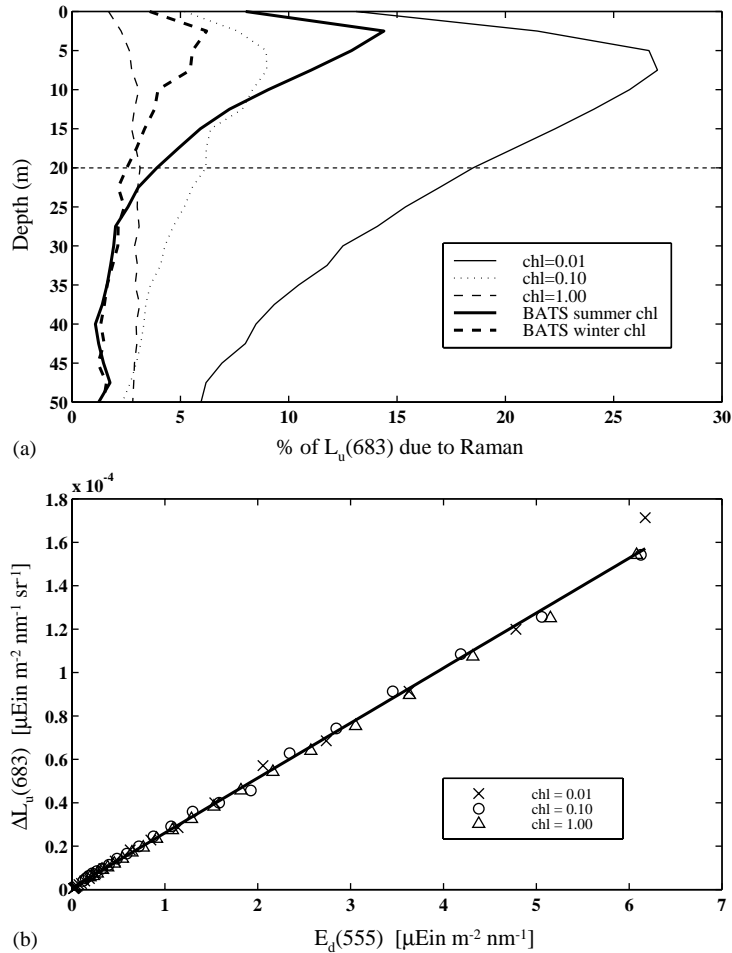


Fig. 2. (a) Percent of $L_u(683, z)$ due to Raman scattering. Values are shown for a range of chlorophyll a concentrations, $chl\ a = 0.01$ (—), $chl\ a = 0.1$ (···), $chl\ a = 1.0$ (---), and using mean BATS profiles for summer (June–Sept., —) and winter (Dec.–Feb., - - -). (b) Linear regression of $\Delta L_u(683)$, the Raman scatter enhancement of $L_u(683)$ versus peak exciting irradiance, $E_d(555)$ evaluated using $chl\ a$ levels from 0.01 to 1.0 mg m^{-3} , fit $r^2 = 0.99$. All values are output from HYDROLIGHT 4.1.

radiance from the two procedures differ by no greater than 10% (Westberry, 2001).

Application of this “correction” to the data has significant effects on the resulting NFR and ϕ_f estimates. Individual profiles of corrected and uncorrected NFR fluxes can differ by 15–60% in the upper 25 m (not shown), but this difference decreases rapidly with depth to only a few percent. On average, Raman scattering accounts for $\sim 30\%$ of the calculated NFR and ϕ_f estimates at 20 m and decreases to 2–3% at depth. These values are very similar to previous estimates

of Raman scattering at 683 nm and suggest that this process must be included in fluorescence studies (Culver and Perry, 1997; Maritorea et al., 2000).

The resulting Raman-corrected upwelling radiances at 683 nm are then used to calculate the daily natural fluorescence flux (NFR) by integration through the solar day as described previously. These values were combined with the daily absorbed flux, AQ, to calculate the quantum yield of fluorescence (Eq. (1a)) at each depth for each cruise.

levels and a deep chlorophyll maximum near 100 m (Fig. 3b). A large degree of interannual variability exists in all environmental variables and has been related to strength of winter mixing (Menzel and Ryther, 1961), community composition changes (Siegel et al., 1990; Steinberg et al., 2001), and other physical forcing mechanisms

(Dickey et al., 1998, 2001). Additionally, the transient mesoscale eddy field has been shown to contribute to the spatial and temporal variability in physical and biogeochemical properties during certain times of year (Doney, 1996; McGillicuddy et al., 1998, 1999; Siegel et al., 1999; Dickey et al., 2001). An overview of the

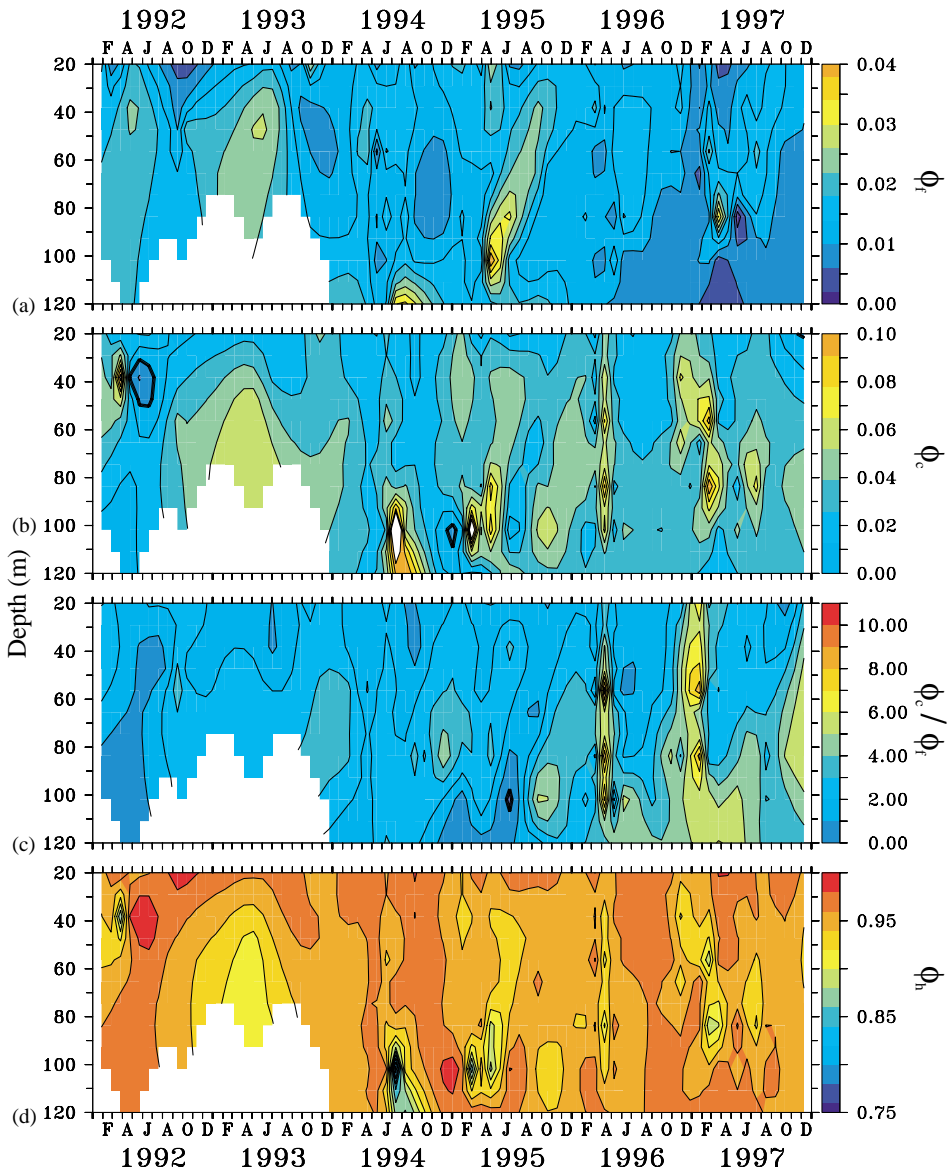


Fig. 4. Time-depth contours of ϕ_f , ϕ_c , ϕ_h and ϕ_c/ϕ_f . Data are calculated at 20, 40, 60, 80, 100, and 120 m and small arrows on x-axis indicate temporal sampling, $N=234$. Values below 80 m were sparse during 1992–1993 because of low sensitivity of the radiometer.

optical and photo-physiological characteristics at the BATS site can be found in Siegel et al. (2001).

The full 6-year time series of ϕ_f , ϕ_c , ϕ_h , and ϕ_c/ϕ_f is shown in Figs. 4a–d for the depth range from 20–120 m. Values of ϕ_f range from nearly zero to ~ 0.05 (or 5%) and fall within the lower range of previous investigations (Kishino et al., 1984; Kiefer et al., 1989; Maritorena et al., 2000). The ϕ_f distribution is very noisy, with episodic highs and lows punctuating the time series (Fig. 4a). Background values are between 0 and 0.02 throughout the year, while the episodic maxima reach greater than 0.04 (4%). Local maxima in ϕ_f are observed at various depths during the late spring and summer, although they are too shallow to be associated with the subsurface chlorophyll maximum.

The pattern is in sharp contrast to the well defined seasonal fluctuations observed in many other physical and biological indices (Figs. 3a–d).

Values of the effective quantum yield of carbon fixation, ϕ_c , range between ~ 0 and 0.125 (mol C/Ein), the theoretical upper bound. These estimates are among the smallest recorded from field observations (Sorensen and Siegel, 2001). Values of ϕ_c also exhibit a large degree of variability, but are generally lower near the surface (mean $\phi_c(20\text{ m})=0.018$) and elevated at depth (mean $\phi_c(120\text{ m})=0.031$) (Table 2). Increases in ϕ_c are observed both in tandem with increases in ϕ_f or independently of its changes. For example, the periods May–Sept. 1994 and April–June 1995 both show significant increases in both quantities at depth, but large increases in ϕ_c during April 1996 and November–January 1997 are unaccompanied

by significant changes in ϕ_f . Consequently, the ratio of the quantum yields, ϕ_c/ϕ_f —which is calculated by dividing the independent estimates of ϕ_f and ϕ_c —reflects both of these patterns. Values of ϕ_c/ϕ_f are generally between zero and 4 (mol C fixed/Ein fluoresced) throughout the time series (Fig. 4c), but a few large values extend the range nearly 3-fold ($0 < \phi_c/\phi_f < 12$). The quantum yield of thermal deactivation ϕ_h is calculated as $1-(\phi_f + \phi_c)$ (Fig. 4d). Patterns in ϕ_h are similar to both ϕ_f and ϕ_c in depth and time. The magnitude of ϕ_h is obviously much greater than that of ϕ_f or ϕ_c and therefore its variability is also much greater (Fig. 5).

Mean and standard deviation of the four quantum yield profiles (Table 2) show relatively little depth dependence of ϕ_f with values between 1% and 2%. However, the mean profile of ϕ_c increases almost two-fold from the surface to 100 m and ϕ_c/ϕ_f shows a near doubling from ~ 2 mol C/Ein at 20 m to ~ 3.5 mol C/Ein at 100 m also. Mean values of ϕ_h are relatively constant with depth (Table 2).

Monthly averages were computed for all four quantities by binning data at 30 day intervals throughout the year (Figs. 6a–d). During the summer, there is a more than 50% decrease in ϕ_f estimates from 0.025 to 0.01 between 20 m and the deepest samples, while the winter period shows more uniform and lower ϕ_f estimates throughout the euphotic zone (Fig. 6a). A significant seasonal cycle is also observed for ϕ_c , as values are consistently reduced during the summer (June–Sept., Fig. 6b). The amplitudes of the seasonal cycles for ϕ_f and ϕ_c are both small relative to the overall variability, accounting for $\sim 5\%$ of the

Table 2
Mean and standard deviation values at each depth for all four quantum yield parameters

Depth (m)	ϕ_f	ϕ_c	ϕ_h	ϕ_c/ϕ_f	<i>N</i>
20	0.0127 ± 0.004	0.0235 ± 0.011	0.964 ± 0.013	2.08 ± 1.07	54
40	0.0152 ± 0.005	0.0351 ± 0.020	0.95 ± 0.021	2.548 ± 1.42	54
60	0.0136 ± 0.005	0.0373 ± 0.021	0.949 ± 0.021	3.166 ± 1.94	46
80	0.0135 ± 0.006	0.0391 ± 0.026	0.946 ± 0.027	3.272 ± 1.98	41
100	0.0128 ± 0.009	0.0427 ± 0.036	0.943 ± 0.043	3.465 ± 2.03	27
120	0.0185 ± 0.008	0.0297 ± 0.031	0.948 ± 0.037	1.846 ± 1.36	8

Data above 20 m has been ignored. Standard deviations are also shown separately in Fig. 5.

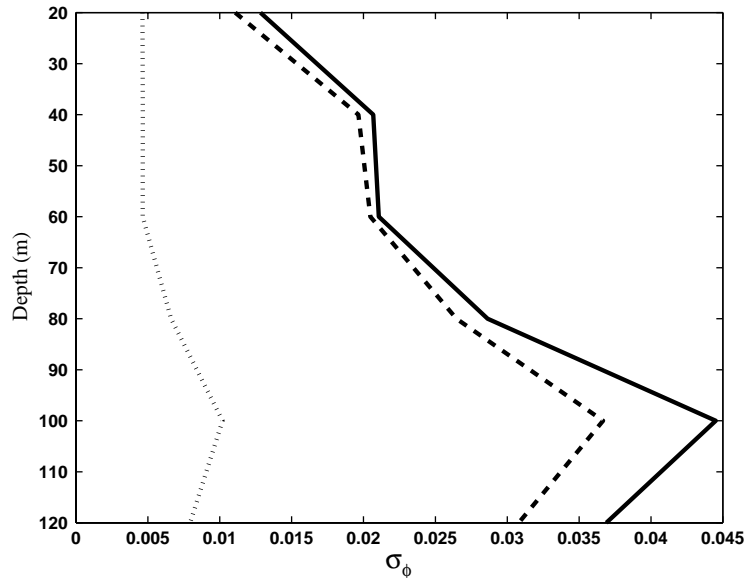


Fig. 5. Standard deviation profiles (1σ) for ϕ_f , ϕ_c - - - - , and ϕ_h ——. Number of samples at each depth are as indicated in Table 2.

total. The seasonal pattern of ϕ_c/ϕ_f shows higher values throughout the upper 100 m (≥ 4 mol C/Ein) in the winter (Dec.–Jan.), while much lower ϕ_c/ϕ_f ratios are found in the summer for the upper 40 m (Fig. 6c). The interior of the euphotic zone (50–90 m) exhibits relatively higher quantum yield ratios during this summer period, decreasing again near 100–120 m. The seasonal cycle for ϕ_c/ϕ_f accounts for $\sim 15\%$ of the overall variability. Large scale seasonal changes in ϕ_h are not apparent.

7. Discussion

7.1. Correlation of quantum yields with environmental variables

The observed variability in the quantum yield properties is quite large and reflects a combination of several physical and physiological factors that can be examined through statistical analyses. Correlation relationships can provide indications of underlying process and can serve as a predictive basis, although some relationships may not have mechanistic meaning. Data were grouped into subsets above and below the level of light

saturation, I_k , in order to separate the effects of light dependence from other environmental controls. Values of I_k were estimated by non-linear least-squares fits to the PP profiles as a function of light (mean depth of $I_k = 36.6 \text{ m} \pm 14.7 \text{ m}$; Siegel et al., 2001). Weak correlations exist between the quantum yield estimates and in situ PAR, day-length, nitrate concentrations, and several pigment indices (Table 3). Many of the correlations are consistent with established ideas about phytoplankton physiology. For example, the strongest correlations (at the 95% confidence level) were found between in situ PAR and ϕ_f , ϕ_c , and ϕ_h . Under light-saturated conditions, both ϕ_f and ϕ_c were inversely related to light intensity while ϕ_h was strongly positively correlated ($r = -0.413$, -0.548 , and 0.585 , respectively). This indicates a role of non-photochemical quenching, whose onset occurs at $\text{PAR}(z) > I_k$ (Kiefer and Reynolds, 1992). This is further supported by the strong positive correlation between ϕ_h and the energy absorbed by photoprotective pigments, $\text{AQ}_{\text{ppc}}(\text{PAR}, z)$ ($\text{Ein m}^{-3} \text{d}^{-1}$) (defined similar to $\text{AQ}(\text{PAR}, z)$ in Eq. (2), but calculated only for photoprotective carotenoids, see Sorensen and Siegel, 2001), all of which is dissipated in the form of heat.

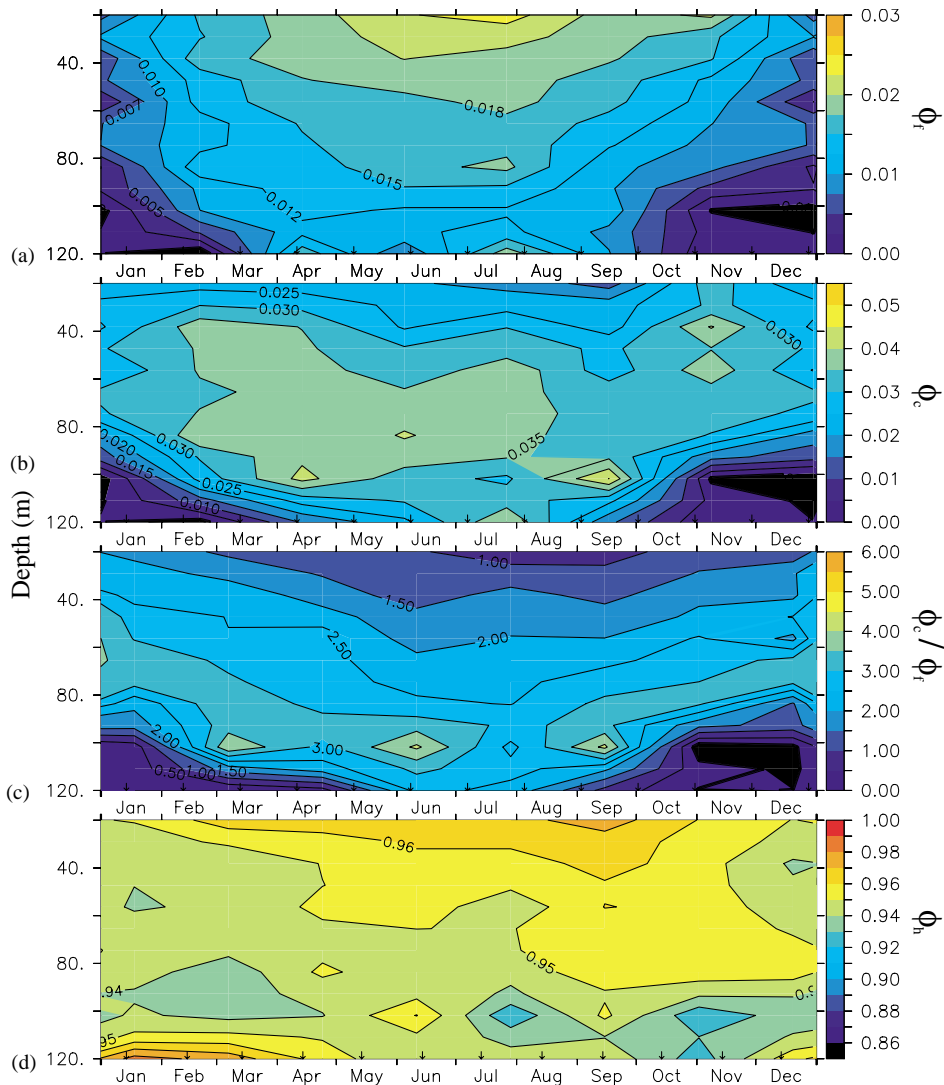


Fig. 6. Monthly averages (1992–1997) of ϕ_f , ϕ_c , ϕ_h and ϕ_c/ϕ_f . Data have been binned at 30 day intervals centered on the middle of each month.

Nutrient effects are difficult to assess in oligotrophic waters because of extremely low concentrations, often below detectability. However, some significant relationships for ϕ_f and nitrate concentration are found. Above I_k , increases in nitrate concentration occur concomitantly with increases in ϕ_f ($r = 0.344$), which one might expect in the absence of photochemical quenching, i.e., in nutrient-poor conditions. Below I_k , this pattern is still found and in addition, a weak but significant inverse relationship between ϕ_c and nitrate con-

centration ($r = -0.163$) appears. This could indicate that although nitrate is present, the phytoplankton community cannot fully utilize those nutrients due to light limitation. This may be the case since the records where nitrate was measurable ($N=107$) were dominated by deep values (~ 100 – 120 m), well below the mean 1% light depth (91 m, Siegel et al., 2001).

Other environmental correlates examined with ϕ_f , ϕ_c , and ϕ_h do show some significant relationships, but do not provide any insight to their

Table 3
Correlation coefficient (r) between quantum yield estimates and environmental variables ($N \sim 230$)

		PP	NO ₃	zeax	chl a	PAR(z)	AQ	AQ _{ppc}	DL
↑ Above I_k	ϕ_f	0.283	0.344	-0.014	0.179	-0.413	-0.125	-0.281	-0.037
	ϕ_c	0.421	-0.101	0.119	0.206	-0.548	-0.358	-0.467	-0.161
	ϕ_h	-0.442	0.014	-0.104	-0.225	0.585	0.350	0.483	0.153
	ϕ_c/ϕ_f	0.242	-0.343	0.154	0.115	-0.360	-0.318	-0.364	0.203
↓ Below I_k	ϕ_f	0.100	0.182	-0.260	-0.269	-0.024	-0.025	-0.025	0.331
	ϕ_c	0.152	-0.163	-0.138	-0.043	-0.287	-0.307	-0.359	-0.109
	ϕ_h	-0.158	0.099	0.185	0.104	0.259	0.276	0.322	0.015
	ϕ_c/ϕ_f	0.052	-0.316	0.127	0.194	-0.300	-0.309	-0.353	-0.386

Correlations are assessed above and below the depth where light saturation occurs, I_k . Numbers in bold indicate significance at the 95% confidence level. PP=primary production, NO₃=nitrate + nitrite, zeax=zeaxanthin, chl a =chlorophyll a , PAR(z)=in situ photosynthetically available radiation, AQ=absorbed quantum energy, AQ_{ppc}=quantum energy absorbed by photoprotective carotenoids, DL=daylength.

behavior. This overall lack of consistent, strong relationships hinders statistical hindcasting of the quantum yields and limits their use for estimating phytoplankton biomass and primary productivity.

7.2. Prediction of PP

The most significant correlations with ϕ_f and ϕ_c were found in relation to in situ PAR, as has been reported in previous work (Kiefer and Reynolds, 1992; Kiefer et al., 1989; Chamberlin et al., 1990). Both ϕ_f and ϕ_c/ϕ_f showed strong negative correlations with PAR(z) which provide the basis for modest predictive success in the quantum yield ratio (Table 3). Chamberlin et al. (1990) quantified this light dependence using a hyperbolic function:

$$\frac{\Phi_c}{\Phi_f}(z) = \frac{k_{cf}}{k_{cf} + \text{PAR}(z)} \left(\frac{\Phi_c}{\Phi_f} \right)_{\max}, \quad (8)$$

where $\phi_c/\phi_{f\max}$ is the maximum ratio of the quantum yields and k_{cf} is the half-saturation constant for ϕ_c/ϕ_f . Chamberlin et al. (1990) report values of 2.3 (mol C/Ein) and 11.49 (Ein m⁻² d⁻¹) for $\phi_c/\phi_{f\max}$ and k_{cf} , respectively, and these values have been applied successfully in a wide variety of environments (Chamberlin and Marra, 1992; Waters and Smith, 1994; Abbott et al., 1995). Using non-linear least-squares fits, BATS/BBOP dataset returned values of 3.73 (mol C/Ein) and 8.6 (Ein m⁻² d⁻¹) for $\phi_c/\phi_{f\max}$ and k_{cf} , (Fig. 7). Both sets of parameters had marginal

success in predicting actual ϕ_c/ϕ_f values and explained only 19% of its variance.

Estimates of PP rates from Eqs. (1a), (1b) and (8) were made by combining the above ϕ_c/ϕ_f results with the NFR values. This approach accounted for ~50% of the variance observed in the BATS depth-dependent PP and in depth integrated rates (mg C m⁻² d⁻¹) (Table 4). Use of the locally optimized fit parameters did not improve the PP hindcasts. Similarly, use of Raman corrected or uncorrected NFR values did not improve the amount of variance explained. Accounting for Raman scatter did, however, significantly reduce the normalized difference between modeled and measured values (Table 4). The performance of this approach for predicting PP rates is slightly better than global bio-optical model predictions for this region (Siegel et al., 2001). Shortcomings likely arise from inaccuracies in ¹⁴C uptake measurements, or “bottle effects” (Peterson, 1980; Balch, 1997) as well as balanced growth assumptions inherent in empirical bio-optical model formulations (Siegel et al., 2001). In addition, the assumptions that ϕ_h is constant and the ratio ϕ_c/ϕ_f is a well behaved function do not appear to be valid in this case.

7.3. Coupling of ϕ_f and ϕ_c

It is commonly assumed that an inverse relationship exists between the pathways of fluorescence

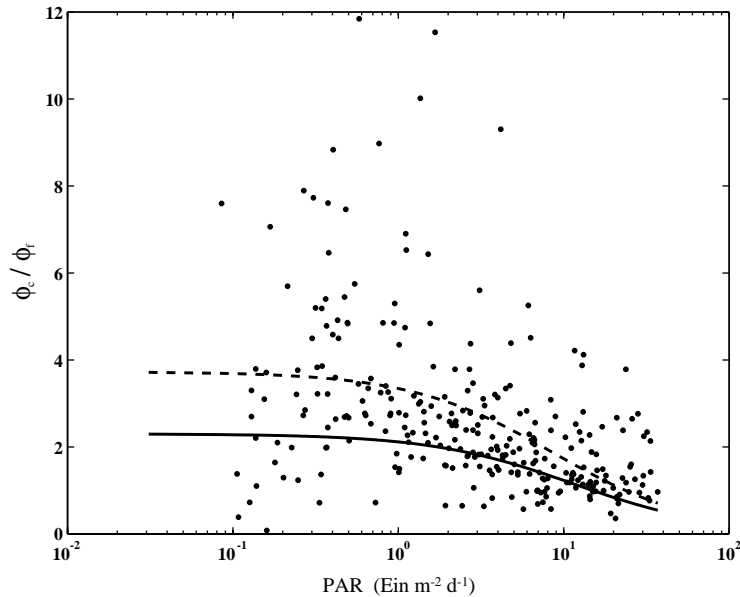


Fig. 7. The ratio ϕ_c/ϕ_f versus in situ PAR, $N=234$. Lines are plotted following Eq. (8), solid line (—) is taken from Chamberlin et al. (1990), dotted line (···) is a non-linear least-squares fit applied to Eq. (8), $r^2 = 19\%$ and 20% , respectively.

Table 4
Prediction success for primary production estimates

	PP(z)		∫PP	
	r^2	% bias	r^2	% bias
BBOP	54%	144	50%	96
w/Raman correction	53%	103	51%	63
Chamberlin et al. (1990)	53%	64	50%	33
w/Raman correction	53%	35	51%	10

Shown are results for depth dependent rates ($N=302$) and water column integrated rates ($N=63$), using both Raman corrected and uncorrected data. % bias is defined as the mean of $(\text{model}-\text{data})/\text{data} \times 100$.

and photosynthesis. This may be appropriate under certain conditions, especially for very short timescales (i.e., seconds to minutes). For example, Letelier et al. (1997) interpreted the decrease in chlorophyll fluorescence efficiency measured by a drifter trapped in a cold-core eddy in the Southern Ocean as the result of nutrient induced, photochemical quenching of fluorescence. More recently, Letelier et al. (2000) suggested increases in ϕ_f in the subtropical Pacific are the result of light limited populations being upwelled and emitting

“excess” absorbed energy as fluorescence. In both of these cases the sampling frequency was able to resolve short-timescale (minutes to days) potential photoadaptive changes. However, only ϕ_f was sampled and the interpretation of the data was based on the assumption of ϕ_f and ϕ_c being inversely related. The data presented here provide an opportunity to examine the coupling between ϕ_f and ϕ_c through direct measurements of PP and NFR. The data and timescales resolved here indicate that some degree of decoupling exists between ϕ_f and ϕ_c on both seasonal and episodic timescales. We calculated anomalies from monthly means for both ϕ_f and ϕ_c on fixed depths (20, 40, ..., 120 m) and used these to examine coupling between the two time series. Fig. 8 shows these anomalies plotted against one another for all depths combined. The data appear evenly or randomly distributed in all four quadrants centered about the intersection of the means (0,0). This suggests that increases or decreases in one quantity do not coincide with increases or decreases of the opposite sign in the other. This is further illustrated by calculating the percentage of time that both anomalies were simultaneously

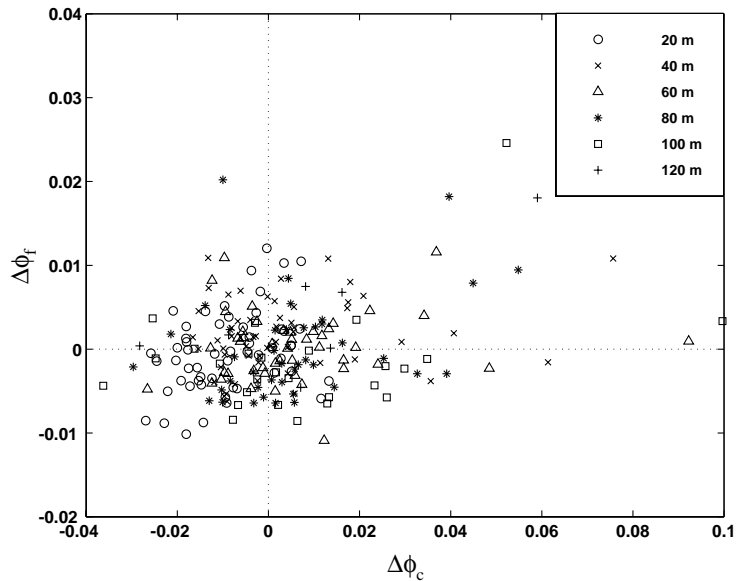


Fig. 8. Anomalies from monthly means of ϕ_f and ϕ_c , $N=234$. Values appear evenly distributed about the centerpoint (0,0) for all depths considered (20–120 m, different symbols for each depth).

greater or less than their respective means and the percentage of time that one quantity was above and one below its mean value. At all depths, it was found that $\sim 50\%$ of the time the quantum yield anomalies were in phase (i.e., both quantities had the same sign) and $\sim 50\%$ of the time the anomalies showed opposite signs. This is an indication that the quantum yields are operating independently of one another.

A more rigorous statistical test to examine the independence of the two time series of monthly ϕ_f and ϕ_c anomalies is a Run Test (Bendat and Piersol, 1986). A “run” was defined as consecutive observations of the same sign (positive or negative), so the greater the number of runs, the greater the degree of independence between the time series. Analogous to the four quadrants in Fig. 6, there are four unique states in which ϕ_f and ϕ_c can occur: both quantities above or below the mean, and one above and the other below its mean value. In all four unique states the time series appear mostly independent (at the 95% confidence level), except for a few cases which were not consistent with depth or any other parameter measured (Table 5).

Table 5

Results from runs tests (Bendat and Piersol, 1986)

Depth (m)	$\Delta\phi_f, \Delta\phi_c$		$\Delta\phi_f, \Delta\phi_c$		$n (=N/2)$
	+, +	-, -	-, +	+, -	
	<i>r</i>	<i>r</i>	<i>r</i>	<i>r</i>	
20	13	32	9	26	27
40	24	21	10	21	2605
60	22	13	8	17	22.5
80	23	17	16	8	20.5
100	7	8	12	7	13.5
120	7	3	2	4	3.5

Number of “runs”, r , for each combination of monthly quantum yield anomalies, $\Delta\phi_f$ and $\Delta\phi_c$ at each depth. Numbers in bold indicate independence ($\alpha = 0.95$).

Fig. 5 also shows that the variance in ϕ_h ($\sim 4.5\%$) is much larger than both ϕ_f and ϕ_c , and has the ability to mask any changes in these quantities. That is, even if an inverse relationship did exist, it might not be realized because of changes in the yield of non-radiative decay processes (Kiefer et al., 1989). The observation that ϕ_h is dynamic on cruise-to-cruise timescales also indicates that an inverse relationship between

ϕ_f and ϕ_c is not assured and reminds us that it must be considered when quantum yield data are applied. Thus, quantum yields of fluorescence and photosynthesis appear to be operating independently of each other, which complicate any parameterization of ϕ_c/ϕ_f .

Acknowledgements

Funding for the BBOP program has been provided by NASA (NAGW-3145), the SeaWiFS project office (NCC-5-49) and NSF (OCE 91-16372 and OCE 90-16990). NSF also supports the core BATS program (OCE 88-01089 and OCE 93-01950). The authors would like to thank the field technicians involved in the BATS/BBOP programs for many years of data collection. Comments from two anonymous reviewers greatly helped the refinement of the manuscript. We are also grateful for many helpful discussions with Tom Dickey, Norm Nelson, Stephane Maritorena, and Curt Mobley, which aided in the development of the manuscript.

References

- Abbott, M.R., Brink, K.H., Booth, C.R., et al., 1995. Scales of variability of bio-optical properties as observed from near-surface drifters. *Journal of Geophysical Research* 100 (7), 13345–13367.
- Austin, R.W., 1974. The remote sensing of spectral radiance from below the ocean surface. In: Jerlov, N.G., Steemann Nielsen, E. (Eds.), *Optical Aspects of Oceanography*. Academic Press, London, pp. 317–344.
- Babin, M., Morel, A., Gentili, B., 1996. Remote sensing of sea surface sun-induced chlorophyll fluorescence—consequences of natural variations in the optical characteristics of phytoplankton and the quantum yield of chlorophyll *a* fluorescence. *International Journal of Remote Sensing* 17 (12), 2417–2448.
- Balch, W.M., 1997. Accuracy of historical primary production measurements. In: *Proceedings of the International Workshop on Oceanographic Biological and Chemical Data Management*, NOAA Technical Report, NESDIS 98, pp. 2279–2293.
- Bannister, T.T., 1992. Model of the mean cosine of underwater radiance and estimation of underwater scalar irradiance. *Limnology and Oceanography* 37, 773–780.
- Bartlett, J.S., Voss, K.J., Sathyendranath, S., Vodacek, A., 1998. Raman scattering by pure water and seawater. *Applied Optics* 37 (15), 3324–3332.
- Bendat, J.S., Piersol, A.G., 1986. *Random Data*. Wiley, New York.
- Berwald, J., Stramski, D., Mobley, C.D., Kiefer, D.A., 1995. Influences of absorption and scattering on vertical changes in the average cosine of the underwater light field. *Limnology and Oceanography* 40 (8), 1347–1357.
- Bidigare, R.R., Ondrusek, M.E., Morrow, J.H., Kiefer, D.A., 1990. In vivo absorption properties of algal pigments. *SPIE* 1302 (Ocean Optics X), 290–302.
- Brody, E.A., 1998. Validation and modeling of in situ inherent optical properties in the Sargasso Sea. Masters thesis, Department of Geography, University of California at Santa Barbara, 108pp.
- Butler, W.L., 1966. Fluorescence yields in photosynthetic systems and its relations to electron transport. In: Sanadi, D.R. (Ed.), *Current Topics in Bioenergetics*, Vol. 1. Academic Press, New York, pp. 49–73.
- Chamberlin, W.S., Marra, J.M., 1992. Estimation of photosynthetic rate from measurements of natural fluorescence: analysis of the effects of light and temperature. *Deep-Sea Research I* 39 (10), 1695–1706.
- Chamberlin, W.S., Booth, C.R., Kiefer, D.A., Marra, J.H., Murphy, R.C., 1990. Evidence for a simple relationship between natural fluorescence, chlorophyll, and photosynthesis in the sea. *Deep-Sea Research I* 37 (6), 951–973.
- Collins, D.J., Kiefer, D.A., SooHoo, J.B., McDermid, I.S., 1985. The role of reabsorption in the spectral distribution of phytoplankton fluorescence emission. *Deep-Sea Research I* 32, 983–1003.
- Culver, M.E., Perry, M.J., 1997. Calculation of solar-induced fluorescence in surface and sub-surface waters. *Journal of Geophysical Research* 102 (5), 10563–10572.
- Dickey, T., Frye, D., Jannasch, H., Boyle, E.A., Manov, D., Sigurdson, D., et al., 1998. Initial results from the Bermuda testbed mooring program. *Deep-Sea Research I* 45, 771–794.
- Dickey, T., Zedler, S., Yu, X., Doney, S., et al., 2001. Physical and biogeochemical variability from hours to years at the Bermuda testbed mooring site: June 1994–March 1998. *Deep-Sea Research II* 48 (8–9), 2105–2140.
- Doney, S.C., 1996. A synoptic atmospheric surface forcing data set and physical upper ocean model for the US JGOFS Bermuda Atlantic Time-Series study site. *Journal of Geophysical Research* 101 (11), 25615–25634.
- Falkowski, P., Kiefer, D.A., 1985. Chlorophyll *a* fluorescence in phytoplankton: relationship to photosynthesis and biomass. *Journal of Plankton Research* 7 (5), 715–731.
- Falkowski, P., Kolber, Z., 1995. Variations in chlorophyll fluorescence yields in phytoplankton in the world oceans. *Australian Journal of Plant Physiology* 22 (2), 341–355.
- Fitzwater, S.E., Knauer, G.A., Martin, J.H., 1982. Metal contamination and its effects on primary production measurements. *Limnology and Oceanography* 27, 544–551.
- Garcia-Mendoza, E., Maske, H., 1996. The relationship of solar-stimulated natural fluorescence and primary productivity in Mexican Pacific waters. *Limnology and Oceanography* 41 (8), 1697–1710.

- Gordon, H.R., 1979. Diffuse reflectance of the ocean: the theory of its augmentation by chlorophyll *a* at 685 nm. *Applied Optics* 18, 1161–1166.
- Gordon, H.R., 1999. Contribution of Raman scattering to water-leaving radiance: a reexamination. *Applied Optics* 38 (15), 3166–3174.
- Gordon, H.R., Voss, K.J., Kilpatrick, K.A., 1993. Angular distribution of fluorescence from phytoplankton. *Limnology and Oceanography* 38 (7), 1582–1585.
- Kiefer, D.A., Reynolds, R.A., 1992. Advances in understanding phytoplankton fluorescence and photosynthesis. In: Falkowski, P.G., Woodhead, A.D. (Eds.), *Primary Productivity and Biogeochemical Cycles in the Sea*. Plenum Press, New York.
- Kiefer, D.A., Chamberlin, W.S., Booth, C.R., 1989. Natural fluorescence of chlorophyll *a*: relationship to photosynthesis and chlorophyll concentration in the western South Pacific gyre. *Limnology and Oceanography* 34 (5), 868–881.
- Kishino, M., Sugihara, A., Okami, N., 1984. Estimation of quantum yield of chlorophyll *a* fluorescence from the upward irradiance spectrum in the sea. *La Mer* 22 (3–4), 233–240.
- Knap, A.H., Michaels, A.F., et al., 1993. BATS Methods—March 1993, BATS Method Manual Version 3. US JGOFS Planning and Coordination Office, Woods Hole, MA.
- Krause, G.H., Weis, E., 1991. Chlorophyll fluorescence and photosynthesis: the basics. *Annual Review of Plant Physiology and Plant Molecular Biology* 42, 313–349.
- Letelier, R.M., Abbott, M.R., 1996. An analysis of chlorophyll fluorescence algorithms for the moderate resolution imaging spectrometer (MODIS). *Remote Sensing of the Environment* 58 (2), 215–223.
- Letelier, R.M., Abbott, M.R., Karl, D.M., 1997. Chlorophyll natural fluorescence response to upwelling events in the Southern Ocean. *Geophysical Research Letters* 24 (4), 409–412.
- Letelier, R.M., Karl, D.M., Abbott, M.R., Flament, P., et al., 2000. Role of late winter mesoscale events in the biogeochemical variability of the upper water column of the North Pacific Subtropical Gyre. *Journal of Geophysical Research-Oceans* 105 (12), 28723–28739.
- Lorenzen, C.J., 1966. A method for continuous measurement of in vivo chlorophyll concentration. *Deep-Sea Research I* 13, 223–227.
- Lohrenz, S.E., Knauer, G.A., Asper, V.L., Tuel, M., Michaels, A.F., Knap, A.H., 1992. Seasonal and interannual variability in primary production and the particle flux in the northwestern Sargasso Sea: US JGOFS Bermuda Atlantic Time Series Station. *Deep-Sea Research I* 39, 1373–1391.
- Maritorena, S., Morel, A., Gentili, B., 2000. Determination of the fluorescence quantum yield by oceanic phytoplankton in their natural habitat. *Applied Optics* 39 (36), 6725–6737.
- Marshall, B.R., Smith, R.C., 1990. Raman scattering and in-water ocean optical properties. *Applied Optics* 29 (1), 71–84.
- McGillicuddy Jr, D.J., Robinson, A.R., Siegel, D.A., Jannasch, H.W., Johnson, R., Dickey, T.D., McNeil, J., Michaels, A.F., Knap, A.H., 1998. Influence of mesoscale eddies on new production in the Sargasso Sea. *Nature* 394, 263–266.
- McGillicuddy Jr, D.J., Johnson, R.J., Siegel, D.A., Michaels, A.F., Bates, N., Knap, A.H., 1999. Mesoscale variability of ocean biogeochemistry in the Sargasso Sea. *Journal of Geophysical Research* 104, 13381–13394.
- Menzel, D.W., Ryther, J.H., 1961. Annual variations in primary production of the sea off Bermuda. *Deep-Sea Research I* 7, 282–288.
- Michaels, A.F., Knap, A.H., et al., 1994. Seasonal patterns of ocean biogeochemistry at the US JGOFS Bermuda Atlantic Time-Series study site. *Deep-Sea Research I* 41 (7), 1013–1048.
- Michaels, A.F., Knap, A.H., 1996. Overview of the U.S. JGOFS Bermuda Atlantic Time-Series Study and the Hydrostation S program. *Deep-Sea Research II* 43 (2–3), 157–198.
- Mobley, C.D., 1994. *Light and Water: Radiative Transfer in Natural Waters*. Academic Press Inc, London.
- Neville, R.A., Gower, J.F.R., 1977. Passive remote sensing of phytoplankton via chlorophyll *a* fluorescence. *Journal of Geophysical Research* 82, 3487–3493.
- O'Brien, M.C., Menzies, D.W., Siegel, D.A., Smith, R.C., 2000. Long-term calibration history of several Marine Environmental Radiometers (MERS). NASA Tech. Memo. SeaWiFS Post-launch Calibration and Validation Analyses 11, 28–48.
- Olaizola, M., La Roche, J., Kolber, Z., Falkowski, P.G., 1994. Non-photochemical quenching and the diadinoxanthin cycle in a marine diatom. *Photosynthesis Research* 41, 357–370.
- Owens, T.G., 1991. Energy transformation and fluorescence in photosynthesis. In: Demers, S. (Ed.), *Particle Analysis in Oceanography*. Springer, Berlin, pp. 101–137.
- Peterson, B.J., 1980. Aquatic primary productivity and the ^{14}C - CO_2 method: a history of the productivity problem. *Annual Review of Ecology and Systematics* 11, 359–385.
- Siegel, D.A., Iturriaga, R., et al., 1990. Meridional variations in the springtime phytoplankton community in the Sargasso Sea. *Journal of Marine Research* 48, 379–412.
- Siegel, D.A., Fields, E., McGillicuddy Jr, D.J., 1999. Mesoscale motions, satellite altimetry and new production in the Sargasso Sea. *Journal of Geophysical Research* 104, 13359–13379.
- Siegel, D.A., Westberry, T.K., O'Brien, M.C., Nelson, N.B., et al., 2001. Bio-optical modeling of primary production on regional scales: The Bermuda Bio-Optics Project. *Deep-Sea Research II* 48, 1865–1896.
- Smith, R.C., Baker, K., 1981. Optical properties of the clearest natural waters. *Applied Optics* 20 (2), 177–184.
- Smith, R.C., Booth, C.R., Star, J.L., 1984. Oceanographic bio-optical profiling system. *Applied Optics* 23, 2791–2797.
- Sorensen, J.C., Siegel, D.A., 2001. Variability of the effective quantum yield for carbon assimilation in the Sargasso Sea. *Deep-Sea Research II* 48, 2005–2035.

- Stavn, R.H., Weidemann, A.D., 1988. Optical modeling of clear ocean light fields: Raman scattering effects. *Applied Optics* 27 (19), 4002–4010.
- Steinberg, D.K., Carlson, C.A., Bates, N.R., Johnson, R.J., Michaels, A.F., Knap, A.H., 2001. Overview of the US JGOFS Bermuda Atlantic Time-Series Study (BATS): a decade-scale look at ocean biology and biogeochemistry. *Deep-Sea Research II* 48, 1405–1447.
- Strickland, J.D.H., Parsons, T.R., 1968. Spectrophotometric determination of chlorophylls and total carotenoids. In: a practical handbook of seawater analysis. Fisheries Research Board of Canada, Bulletin 167, 185–192.
- Topliss, B.J., Platt, T., 1986. Passive fluorescence and photosynthesis in the ocean: Implications for remote sensing. *Deep-Sea Research I* 33, 849–864.
- Waters, K.J., Smith, R.C., 1994. Phytoplankton production in the Sargasso Sea as determined using optical mooring data. *Journal of Geophysical Research* 99 (9), 18385–18402.
- Westberry, T., 2001. Phytoplankton natural fluorescence variability and primary production in the Sargasso Sea. Masters thesis. Interdepartmental Program in Marine Science, University of California, Santa Barbara, 65pp.